






ARTICLE

The N2A region of titin has a unique structural configuration

Chiara Stronczek¹, Stephan Lange^{2,3}, Belinda Bullard⁴, Sebastian Wolniak¹, Emma Börgeson³, Olga Mayans¹, and Jennifer R. Fleming¹

The N2A segment of titin is a main signaling hub in the sarcomeric I-band that recruits various signaling factors and processing enzymes. It has also been proposed to play a role in force production through its Ca²⁺-regulated association with actin. However, the molecular basis by which N2A performs these functions selectively within the repetitive and extensive titin chain remains poorly understood. Here, we analyze the structure of N2A components and their association with F-actin. Specifically, we characterized the structure of its Ig domains by elucidating the atomic structure of the I81-I83 tandem using x-ray crystallography and computing a homology model for I80. Structural data revealed these domains to present heterogeneous and divergent Ig folds, where I81 and I83 have unique loop structures. Notably, the I81-I83 tandem has a distinct rotational chain arrangement that confers it a unique multi-domain topography. However, we could not identify specific Ca²⁺-binding sites in these Ig domains, nor evidence of the association of titin N2A components with F-actin in transfected C2C12 myoblasts or C2C12-derived myotubes. In addition, F-actin cosedimentation assays failed to reveal binding to N2A. We conclude that N2A has a unique architecture that predictably supports its selective recruitment of binding partners in signaling, but that its mechanical role through interaction with F-actin awaits validation.

Introduction

Titin contains several mechanosignaling hubs that act to scaffold and organize mechanoresponsive signaling elements (Henderson et al., 2017). One of these, the N2A component, is located within the I-band region of titin, immediately N-terminal to the PEVK spring (Fig. 1 A; LeWinter and Granzier, 2010). Titin is differentially spliced into different isoforms with and without the N2A component. The titin N2A isoform, which takes its name from this element, is the predominant isotype in skeletal muscle cells. However, the N2A element is also present in the titin N2BA isoform expressed in cardiac muscle (Cazorla et al., 2000). The N2A region is composed of four Ig domains (I80, I81, I82, and I83) and a unique sequence of ~100 residues (UN2A) inserted between domains I80 and I81 (Fig. 1 A). The UN2A insert has been found to have an α -helical structural content (Zhou et al., 2016; Tiffany et al., 2017). Titin N2A acts as a protein interaction node that recruits several regulatory proteins and stress response factors to the sarcomere. Of these, the interaction with muscle ankyrin repeat proteins (MARPs) is the best characterized to date, in particular with the cardiac ankyrin repeat protein (CARP) member of this family,

which has been shown to bind the UN2A-I81 fraction of N2A (Miller et al., 2003; Lun et al., 2014; Zhou et al., 2016). Additionally, the SET and MYND-containing lysine methyltransferase 2 (SMYD2) has also been identified as a UN2A binder (Donlin et al., 2012). The P94/calpain3 protease binds I80-UN2A and also across I82-I83 stretching into the PEVK region (Hayashi et al., 2008). Currently, the molecular basis of these titin interactions and their regulatory principles remain poorly characterized.

Titin N2A is also suspected to play a mechanical role in the sarcomere. The titin protein is known to contribute passive force to the sarcomere and to maintain its structural integrity (Granzier and Labeit, 2004). Titin's role in passive force resides in the extensibility of its I-band region, where first its tandem-Ig section and then its PEVK region extend serially in function of stretch (Trombitás et al., 1998). More recently, titin has been thought to also play a role in active force development, possibly by intervening in length-dependent activation in a calcium-dependent manner (Hessel et al., 2017). The exact mechanisms by which titin might lead to an increase in length-dependent

¹Department of Biology, University of Konstanz, Konstanz, Germany; ²Division of Cardiology, School of Medicine, University of California, San Diego, San Diego, CA; ³Wallenberg Laboratory, Department of Molecular and Clinical Medicine, Institute of Medicine, University of Gothenburg, Gothenburg, Sweden; ⁴Department of Biology, University of York, York, UK.

Correspondence to Jennifer R. Fleming: Jennifer.fleming@uni-konstanz.de

This work is part of a special collection on myofilament function and disease.

© 2021 Stronczek et al. This article is distributed under the terms of an Attribution–Noncommercial–Share Alike–No Mirror Sites license for the first six months after the publication date (see <http://www.rupress.org/terms/>). After six months it is available under a Creative Commons License (Attribution–Noncommercial–Share Alike 4.0 International license, as described at <https://creativecommons.org/licenses/by-nc-sa/4.0/>).

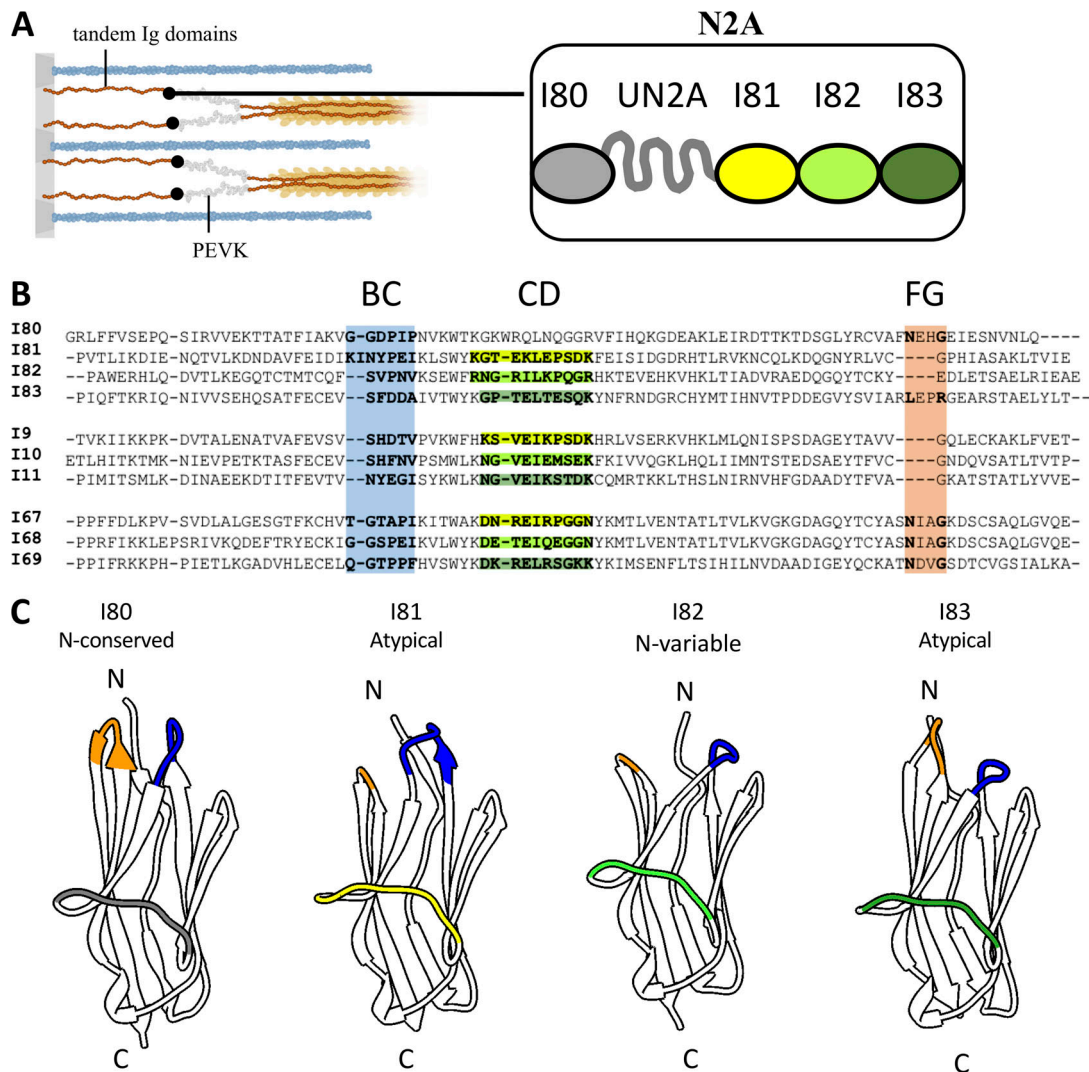


Figure 1. **N2A location and Ig domain components of titin N2A with their unique loop features.** (A) Left: Location of N2A in the sarcomere. Thin filaments shown in blue; thick filaments in yellow; Z-line gray rectangle. Titin's tandem domains are orange and the PEVK is gray. Right: Domain composition of the N2A region. (B) Alignment of human titin sequences of N2A Ig domains (I80-I83) and representative domains from constitutive (I19-I11) and skeletal (I167-I169) tandems. BC loops are highlighted in blue, FG β -hairpin in orange, and CD loops in shades of green. (C) Ig domain components of the N2A region. I81, I82, and I83 domains are as elucidated crystallographically in this work; I80 was modeled using I-TASSER (Yang and Zhang, 2015). Ig domains are shown in cartoon representation, with BC, CD, and FG loop features colored as in B. C, C terminus; N, N terminus.

active force production remain a subject of debate. In this respect, titin-based passive stiffness has been shown to affect the calcium sensitivity of force through myofilament lattice spacing effects, whereby the structure of the thick filaments is altered, affecting the activation of cross-bridges and the production of active force (Cazorla et al., 2001; Lee et al., 2013). The molecular mechanisms underlying this phenomenon are not fully understood, although it has been proposed that titin could form a calcium-dependent association with actin to oppose shortening during contraction (Hessel et al., 2017). In this regard, the calcium-dependent association of titin with both filamentous actin (F-actin) and reconstituted thin filaments has been observed (Kellermayer and Granzier, 1996). Molecularly, titin's PEVK region has been shown to associate with F-actin, thereby elevating passive tension in skinned myofibrils (Yamasaki et al., 2001). PEVK is highly charged and minimally structured, being

known to bind calcium, which regulates its molecular spring properties (Labeit et al., 2003). Lately, the titin N2A component has also been proposed to form a calcium-enhanced association with F-actin based on in vitro, single-molecule, atomic force spectroscopy data (Dutta et al., 2018; Nishikawa et al., 2019). This association could affect the extensibility of titin's I-band region, in particular its proximal Ig-tandem, by pinning the N2A to the thin filament. In view of a recent biochemical study that showed domain I83 to be poorly stable but to become stabilized by calcium (Kelly et al., 2020), it was then hypothesized that I83 might be central to mediate the calcium-regulated titin-N2A/F-actin interaction (Nishikawa et al., 2020). A potential role of I83 in active force production has been further supported by data from the *mdm* mouse. These mice contain a deletion that removes the final two β -strands of domain I83 as well as a small portion of the PEVK region (Garvey et al., 2002). This results in a

severe muscle dystrophy phenotype (Garvey et al., 2002), with a three- to fourfold decrease in force production during active stretch (Powers et al., 2016; Tahir et al., 2020). The mice also show disruption of the N2A signaling pathways (Garvey et al., 2002; Witt et al., 2004; Huebsch et al., 2005). Given these observations, a need now exists to unravel the molecular basis of titin N2A's contributions to sarcomere signaling and mechanics.

To determine how the seemingly innocuous, highly conserved Ig domain components of titin N2A can function as a selective protein interaction node, and how this could contribute to the mechanical function of titin, we elucidated the atomic structure of the I81-I83 Ig tandem and examined the model to probe its capability to bind calcium specifically. Further, we tested the existence of a titin-N2A/F-actin interaction using *in vitro* cosedimentation assays in the presence and absence of calcium, as well as transfection studies in C2C12 myoblastoma cells and C2C12-derived myotubes. The results identified distinct features in the 3-D structure of I81-I83 that may explain its ability to be specifically recognized by the binding partners of the N2A locus. However, we found no evidence of specific calcium-binding sites and also no evidence of a direct association of titin N2A and F-actin. Our findings highlight the unique scaffolding potential of N2A as signaling node, but do not bring support to its direct role in active force production through an association with F-actin.

Materials and methods

Protein production

I81-I83 from human titin (residues 9582–9851; Uniprot accession no. Q8WZ42; to ease structural annotation, residue P9582 is taken as residue P1 when describing the crystal structure) was cloned into the vector pETM-11 (European Molecular Biology Laboratory collection) using NcoI and KpnI restriction sites. The pETM-11 vector adds a His₆-tag and a tobacco etch virus cleavage site N-terminally to the inserted gene.

Protein samples were produced in *Escherichia coli* Rosetta (DE3; Merck Millipore) cultivated at 37°C in Luria-Bertani medium supplemented with kanamycin (100 µg/ml) and chloramphenicol (33 µg/ml). At an OD₆₀₀ = 0.6, expression was induced with 0.5 mM isopropyl-β-D-1-thiogalactopyranoside, and cultures were grown further overnight at 18°C. Cells were harvested by centrifugation and lysed by sonication in buffer A (40 mM Tris-HCl, pH 8.0, 300 mM NaCl, 20 mM imidazole, and 1 mM dithiothreitol [DTT]) in the presence of an EDTA-free protease inhibitor cocktail (Roche Applied Science). Lysates were clarified by centrifugation (40,000 g, 4°C, 40 min). I81-I83 was then isolated from the supernatant by Ni²⁺-affinity chromatography on a HisTrap HP 5-ml column (GE Healthcare). Elution used a linear gradient of imidazole (20–500 mM). Next, the affinity tag was removed by overnight incubation with tobacco etch virus protease while in dialysis against buffer A. Tag and protease were removed using subtractive affinity chromatography, and the sample was further dialysed into buffer B (20 mM Tris-HCl, pH 8.0, 100 mM NaCl, and 1 mM DTT). The resultant sample was subjected to size exclusion chromatography on a Superdex S75 16/60 column (GE Healthcare)

preequilibrated in buffer B. The purity of the sample obtained was assessed to be 99% by SDS-PAGE. The sample was flash-frozen in liquid nitrogen and stored at –80°C until further use.

Recombinant UN2A-I81 (residues 9472–9581; UniprotKB Q8WZ42) was produced as described above for I81-I83, except that the buffer system used was 25 mM HEPES, pH 7.5, with no DTT.

Crystal structure determination

I81-I83 was crystalized at 20°C on 96-well Intelliplates (Art Robbins Instruments) using sitting drops (400 nl total drop volume) containing equal volumes of protein (31 mg/ml) and reservoir solutions (25% [wt/vol] polyethylene glycol 3350, 100 mM bis-Tris, pH 5.5, and 200 mM lithium sulfate).

For x-ray data collection, crystals were cryoprotected with mother liquor supplemented with 30% [vol/vol] ethylene glycol before vitrification in liquid nitrogen. X-ray diffraction data were collected at the Swiss Light Source synchrotron and processed using the XDS suite (Kabsch, 2010). Molecular replacement was conducted with Phaser (McCoy et al., 2007) using a version of the single Ig domain I81 (Protein Data Bank [PDB] accession no. 5JOE; Zhou et al., 2016) as search model, where BC and FG loops had been manually truncated. The search model corresponded to one twelfth (~8%) of the crystallographic asymmetric unit. Initial automated model building was performed using the warpNtrace routine within ARP/wARP (Lamzin et al., 2012). Manual model building was performed in Coot (Emsley and Cowtan, 2004), and refinement used PHENIX (Adams et al., 2010). Refinement included noncrystallographic symmetry restraints and per-domain Translation/Libration/Screw (TLS) model of rigid-body harmonic displacements treatment. Model quality was assessed using MolProbity (Williams et al., 2018). Diffraction data and model statistics are given in Table 1. X-ray diffraction images have been deposited in Zenodo (Fleming, 2021). Structure factor amplitudes and model coordinates are deposited in the PDB under accession no. 7AHS.

Bioinformatic analysis of I81-I83 crystal structure

To identify possible calcium binding sites in I81-I83, chain A of the crystal structure was stripped from solvent atoms and analyzed using the IonCon (Hu et al., 2016) and Metsite (Sodhi et al., 2004) algorithms and the search restricted to calcium ions. For Metsite, false rate cutoffs of 1, 5, 10, and 20% were tested. Metsite uses an artificial neural network trained using all protein chains interacting with the specified metal ions from the PDB and clustering at a 25% sequence identity. The following classifying features were used to train the artificial neural network: sequence profile information, secondary structure, solvent accessibility, and distance matrices of site residues. Ioncon uses a support vector machine trained on sequence profiles, local structure properties (including solvent accessibility), and position- and segment-specific conservation scores of a nonredundant set of ion-binding proteins from the BioLiP database (Yang et al., 2013), which have a pairwise sequence identity <30%. Although there is some overlap between the input classifier types, and possibly training datasets, each approach uses its own machine learning technique and weightings and

Table 1. X-ray diffraction data processing statistics and model refinement parameters

PDB accession no.	7AHS
Space group	$P2_12_12_1$
Cell dimensions	
$a, b, c, \text{Å}$	85.20, 87.34, 161.58
$\alpha, \beta, \gamma, ^\circ$	90, 90, 90
Molecules in asymmetric unit	4
X-ray data	
X-ray source	SLS PX III
Detector	PILATUS 2MF
Wavelength, Å	1.00003
Resolution, Å	43.67-2.05 (2.1-2.05)
Unique reflections	76,413 (5,256)
Multiplicity	13.4 (12.8)
Completeness (%)	100 (100)
$\langle I/\sigma(I) \rangle$	13.45 (1.18)
R_{meas} (%)	19 (236)
$CC_{1/2}$ (%)	99.9 (37.6)
Refinement	
Reflections work/R-free sets	74,495/1,841
Protein atoms/waters	8,884/1,004
Ligands	EDO \times 11, GOL \times 1, SO ₄ \times 6
$R_{\text{factor}}/R_{\text{free}}$, %	18.3/23.5
RMSD bond length, Å/angle, °	0.009/1.215
Ramachandran favored/outliers, %	97.50/0.19

Values in parentheses are for the highest resolution shell. EDO, ethylene glycol; GOL, glycerol; SO₄, sulfate. (h, i) . $R_{\text{work}} = \sum hki ||F_o| - |F_c|| / \sum |F_o|$, where F_o is the observed structure factor amplitude and F_c is the structure-factor amplitude calculated from the model. R_{free} is the same as R_{work} except that it was only calculated using a subset, 5%, of the data that are not included in any refinement calculations. R_{meas} , defined as $R_{\text{meas}} = \sum (n_h/n_h - 1)^{1/2} \sum_i |I_{h_i} - I_{h_i}| / \sum_h \sum_i I_{h_i}$, where n_h denotes multiplicity. $CC_{1/2} = \frac{\sigma_{\text{obs}}^2}{\sigma_{\text{calc}}^2} = \frac{\sigma_{\text{obs}}^2 - \sigma_{\text{e}}^2}{\sigma_{\text{calc}}^2 - \sigma_{\text{e}}^2}$. This requires calculation of σ_{v}^2 , the variance of the average intensities, and σ_{e}^2 , the average of the variances of the averaged (merged) intensities.

descriptions of classifications, making them complementary methods. Critically, both methods use 3-D structural information in their molecular analysis. In addition, the distribution of surface charges was calculated and visualized using UCSF Chimera (Pettersen et al., 2004). The Coulombic Surface Electrostatic potential was calculated according to Coulomb's law using the function Coulombic Surface Coloring with a distance-dependent dielectric constant (ϵ) of 4.0, a solvent-accessible surface cutoff of 1.4 Å, and histidine residues implicitly protonated. Default grid settings were used.

Actin cosedimentation

Actin was prepared from rabbit back muscle (Spudich and Watt, 1971). G-actin was centrifuged at 100,000 g for 30 min, and the

supernatant was polymerized in 50 mM NaCl, 20 mM MOPS, pH 7.0, and 5 mM MgCl₂. Titin I81-I83 and UN2A-I81 samples were centrifuged at 100,000 g for 30 min immediately before the assay. Titin UN2A-I81 or I81-I83 (20 μ M) was added to actin (10 μ M). Assay buffers were 50 mM NaCl, 20 mM MOPS, pH 7.0, and 5 mM MgCl₂, with either 2 mM CaCl₂ or 2 mM EGTA. Samples were incubated at 23°C for 1 h and centrifuged at 100,000 g for 30 min. Supernatant and pellet fractions were analyzed by SDS-PAGE with 12% acrylamide gels stained with Coomassie Brilliant Blue-G-250.

Protein expression and localization in C2C12 cells

For cellular studies, human titin fragments I80-UN2A-I81 (residues 9353-9671; UniprotKB accession no. Q8WZ42) and I81-I83 (residues 9582-9851; UniprotKB accession no. Q8WZ42) were amplified by PCR and subcloned in frame into mammalian expression vectors encoding fluorescent proteins N-terminally to the target insert, pEGFP-C1 (Clontech) or mCherry-C1. In the latter plasmid, the GFP encoded in pEGFP-C1 was replaced by mCherry. All constructs were confirmed by sequencing.

Mammalian expression constructs were then transfected into C2C12 cells (American Type Culture Collection) using Lipofectamine 2000 (Thermo Fisher Scientific) as previously described (Lange et al., 2012). Following 2 or 7 d of differentiation, cells were fixed with 4% paraformaldehyde in PBS for 5 min at room temperature. Cells were permeabilized using 1 \times PBS supplemented with 0.2% Triton X-100 for 5 min, and subsequently stained with a knockout-validated primary antibody against the sarcomeric protein obscurin (region covering IQ-Ig64; Blondelle et al., 2019) for 2 h at room temperature. Following three washes with 1 \times PBS for 5 min each, cells were stained for 1 h with a rabbit secondary antibody linked to either Alexa-488 or Alexa-594 (Jackson ImmunoResearch; 711-545-152 and 711-585-152) and Alexa-647 phalloidin (Thermo Fisher Scientific; A22287) dissolved in gold buffer (20 mM Tris-HCl, pH 7.5, 155 mM NaCl, 2 mM ethylene glycol tetraacetic acid, 2 mM MgCl₂, and 5% BSA). Alexa-647 phalloidin stained F-actin. After washing cells three times with 1 \times PBS, cells were mounted in fluorescent mounting medium (ProLong Gold antifade reagent; Invitrogen) and processed for imaging on a Leica SP5 confocal microscope in sequential scanning mode using a 63 \times oil-immersion objective and zoom rates between 1 and 4. Images were analyzed using ImageJ and the BioFormats Importer as well as Photoshop (Adobe).

Results

The crystal structure of I81-I83 reveals distinct molecular features

The I81-I83 tandem from titin has been proposed to be central to the calcium-dependent association of titin and F-actin at the N2A sarcomeric locus, with domain I83 suspected to be the key mediator of this interaction (Dutta et al., 2018; Nishikawa et al., 2019). As titin is a repetitive multi-Ig chain where component domains are highly homologous, we aimed to reveal the distinct molecular features of I81-I83 that could confer it the ability of mediating specific interactions and of coordinating calcium. For

this, we elucidated the 3-D structure of I81-I83 from human titin to 2.05 Å resolution using x-ray crystallography (Table 1). The crystal used in this study contained four molecular copies of I81-I83 in its asymmetric unit. These copies consistently revealed I81-I83 as a monomeric chain with an extended domain arrangement. Copies of individual domains were essentially identical across the four replicas (RMSD values: I81 = 0.68–0.98; I82 = 0.36–0.40; and I83 = 0.50–0.47). At the tandem level, the molecular copies were also highly similar, revealing only a minor deviation of 35° along the longitudinal molecular axis as a result of crystal packing. Overall, the four crystalline copies were in full agreement.

First, we examined the structure of the individual domains I81, I82, and I83 to assign them to established Ig fold subclasses in titin. Titin Ig domains have been classified into “N-conserved” and “N-variable” types according to the features of the loop cluster at the N-terminal side of their fold (Marino et al., 2005). In brief, N-conserved domains have a lengthened Ig fold characterized by the presence of (i) a PPxf motif at the N-terminal β-strand A; (ii) a lengthened FG β-hairpin housing a conserved NxxG motif; and (iii) an extended BC loop containing proline residues that often form a PPh (h, hydrophobic residue) or PxP motif, where at least one proline adopts a cis conformation. β-strand A, BC loop, and FG β-hairpin cluster tightly at the N-terminal side of the Ig fold, with prolines in β-strand A and BC loop stacking together and the asparagine residue in the NxxG sequence of the FG β-turn forming a crucial hydrogen bond to the BC loop that secures the mutual packing. N-variable Ig domains lack these features and are shorter in length, defined by short BC and FG elements and a β-strand A that is variable in sequence. Canonical representatives of the N-conserved subclass are the Ig domains of the differentially spliced, skeletal I-band tandem (e.g., I65-I70; von Castelmur et al., 2008), while typical members of the N-variable subclass form the constitutive I-band tandem (e.g., I9-III; Bogomolovas et al., 2016). A structural and sequence comparison of I81, I82, and I83 with classified titin domains of known 3-D structure revealed that I82 is a typical member of the N-variable titin subclass, while I81 and I83 display distinct features in that their BC loops and FG β-turns are mismatched (Fig. 1, A and B). I81 has a long BC loop but a short FG β-hairpin (Zhou et al., 2016), while contrarily I83 has a short BC loop but an extended FG β-hairpin. The different length of these loops in I81 and I83 causes them to no longer pack against each other. This releases the constraints in sequence composition. In I81 the BC loop is atypically long, even one residue longer than the typical N-conserved Ig type. In I83, the FG β-turn now contains an atypical LEPR motif (instead of the canonical NxxG motif), and the short BC loop lacks prolines (Fig. 1 B). In the position of β-strand A, which normally is an integral component of the ABDE β-sheet, both I82 and I83 possess instead a β-bulge that protrudes from the surface of the domain. Whether this feature is also important to allow for recognition of specific protein partners bears further investigation.

To complete the analysis of Ig domain components of titin N2A, we analyzed the sequence of I80 and performed its homology modeling using I-TASSER (Yang and Zhang, 2015) and Phyre-2 (Kelley et al., 2015). Based on sequence features and supported by 3-D models, we concluded that I80 displays canonical features of the N-conserved subclass (Fig. 1, A and B). This is the class of

the majority of I-band Igs. Unlike I81 and I83, it does not show novel features.

In summary, our findings reveal that titin N2A is composed of heterogeneous Ig domains, where I80 and I82 belong to N-conserved and N-variable types, respectively, and I81 and I83 present unique, individual loop structures (Fig. 1 B).

I81-I83 display a unique tandem architecture

In titin, Ig domains are linked in series connected by short linker sequences, thereby forming domain tandems. Available crystal structures of titin Ig tandems (reviewed in Zacharchenko et al., 2015) have revealed that these normally adopt an extended chain conformation, where Ig-Ig interfaces show few direct contacts. Interestingly, 3-D structures also show that the tandems display local rotational order along their longitudinal chain axes. Such rotational order is largely a steric consequence of the BC loop and FG β-hairpin features of the individual Ig in the tandem, as such loops form the Ig-Ig interfaces (Fig. 2 A). The skeletal I-band tandem composed of N-conserved Ig domains with elongated BC and FG features shows a characteristic up-down arrangement, where individual Igs are rotated 180° with respect to each other along the chain (Fig. 2, B and C; von Castelmur et al., 2008). On the other hand, the constitutive I-band tandem, which is composed of short N-variable Ig domains, shows slight domain rotations of 45–68° angles (Fig. 2, B and C; Bogomolovas et al., 2016). The N2A tandem I81-I83 shows individual Igs arranged at a 90° angle with respect to one another, which results from the hybrid loop features of its component domains (Fig. 2 C). The interfaces between these domains in N2A are restrained (Fig. 2 A). The I81-I82 interface shows hydrogen bonds from the domains to the linker (I81-K15 to linker E90 and I82-S115 to linker V116) as well as a hydrophobic patch (I81-L14, I81-I89, and I82-V116). The hydrophobic patch will energetically prevent the rotation of the interface, while the hydrogen bonds stabilize it. The interface I82-I83 is also restrained with a direct salt bridge (I82-E104 to I83-R258), among other stabilizing hydrogen bonds (I82-R258 to linker P179). Interestingly, this reveals that the N2A tandem not only displays individualized features at the local domain level but also has a unique overall 3-D chain topography that is distinct from that of other Ig tandems in titin’s I-band.

No specific calcium binding sites can be identified in I81-I83

The crystal structure of I81-I83, which includes its solvent molecules (Table 1), did not reveal any divalent ions according to experimental electron density values. Thus, in order to identify possible calcium binding sites in I81-I83, the topography of its electrostatic surface potential was investigated using bioinformatic tools. For identified negatively charged surface loci, the geometry of surface amino acids was inspected to evaluate their capability to coordinate divalent metals. For the specific coordination of a calcium ion by a protein, the protein surface must offer a negatively charged pocket with a minimum of four planar coordinating atoms. Six coordinating atoms are more commonly observed and eight coordinating atoms are seen in high-affinity calcium binding sites in proteins (Katz et al., 1996). Common calcium-coordinating residues are the side chains of residues Asp and Glu, with Asn, Gln, Ser, and Thr possible but less frequently observed (Hu et al., 2016; Katz et al.,

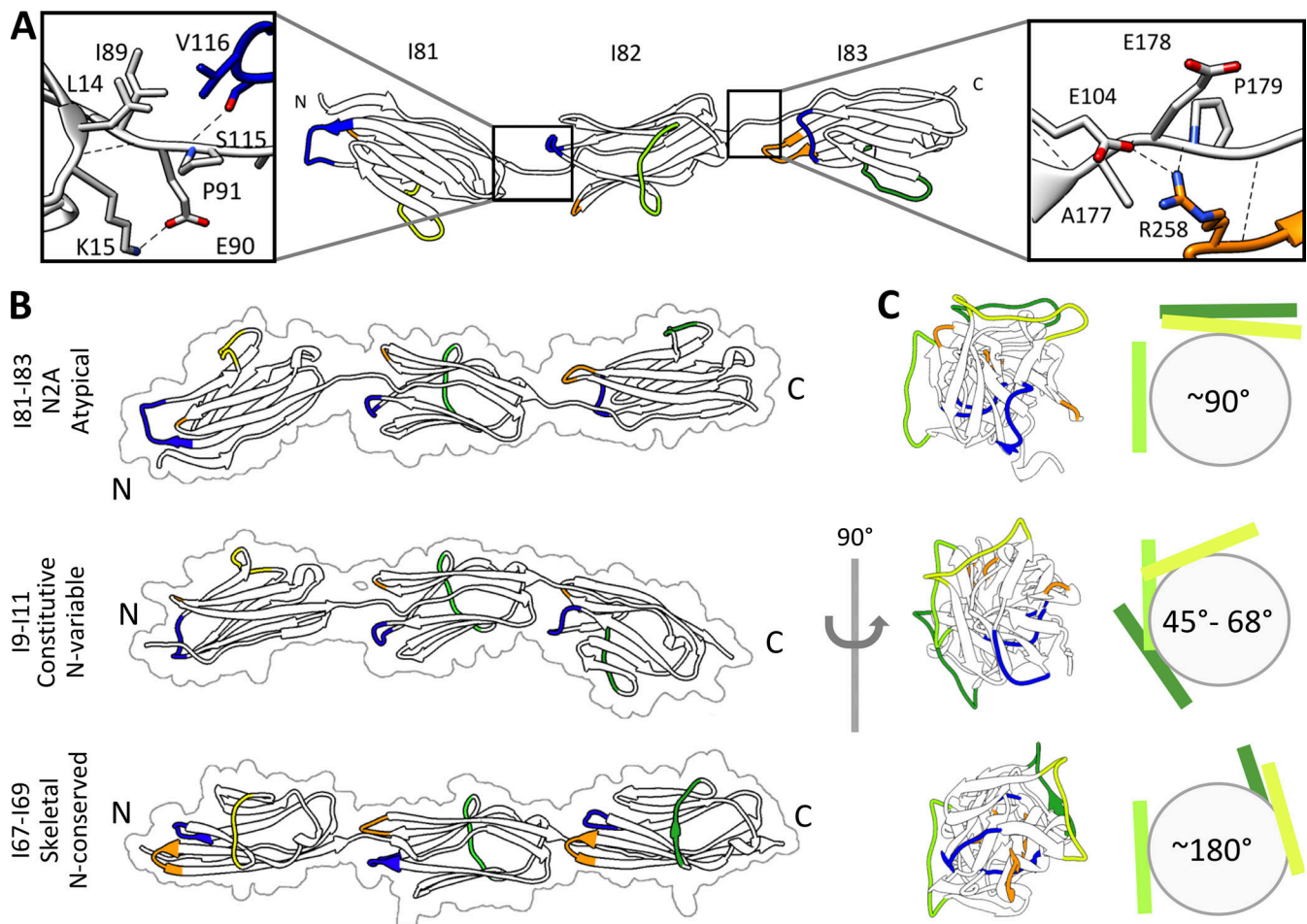


Figure 2. **Domain interfaces create a unique tandem architecture.** (A) Residues involved in interdomain interactions are shown as sticks colored by atom type (N, mid-blue; O, red; C, as regions shown in Fig. 1, where the FG loop is orange, the BC loop is royal blue, and all other regions are white). Hydrogen bonds are shown as dashed lines. (B) Comparison of chain architecture in titin Ig tandems from N2A (I81-I83), constitutive (I9-I11; PDB accession no. 5JDD), and skeletal (I67-I69; PDB accession no. 2RIK) I-band regions. Structures are shown as cartoon ribbons with the surface shown as gray underlay. BC, CD, and FG features are colored as in A. To facilitate visual comparison, structures are displayed so that the middle Ig domain adopts a same orientation (C) View along the longitudinal molecular axis showing the relative orientation of domains in each tandem. Left as a cartoon ribbon and right as a schematic where the domains are a circle and the CD loops are represented as lines. BC, CD, and FG features are colored as in A. C, C terminus; N, N terminus.

1996). Additionally, main chain oxygens and water molecules can contribute to the calcium ion's coordination (Katz et al., 1996). An examination of the crystal structure of I81-I83 showed that, despite the existence of negatively charged surface regions (red areas, Fig. 3), no surface residue clusters satisfy those requirements, even when considering alternative side-chain rotamer rearrangements. To further confirm the lack of calcium sites, the structure was submitted to two independent structure-based metal binding predictor servers: IonCom (Hu et al., 2016) and Metsite (Sodhi et al., 2004). No calcium binding sites were found by these servers. We therefore concluded that I81-I83 as here observed is unlikely to bind calcium specifically and with high affinity.

Titin N2A components do not colocalize with F-actin in C2C12 cells

To investigate if the particular characteristics of I81-I83 mediate an interaction with F-actin, we studied the localization of the titin N2A constructs I80-UN2A-I81 and I81-I83 in transfected C2C12 muscle cells. For this, I80-UN2A-81 or I81-I83 fused C-terminally to

the fluorescent proteins GFP or mCherry was transfected into C2C12 myoblasts and actin-stained with Alexa-647 phalloidin to investigate the respective subcellular localizations. In cells differentiated for 2 d, I80-UN2A-I81 and I81-I83 both displayed a diffuse localization (Fig. 4 A), with I81-I83 also showing nuclear enrichment and forming a few cytoplasmic puncta (Fig. 4 A, right). Neither titin fragment displayed an association with actin filaments. However, F-actin during early differentiation of C2C12 myoblasts may still incorporate the nonmuscle β -actin isotype, and may not be decorated with sarcomeric proteins seen in the thin filaments of mature muscle fibers. Hence, to account for actin isotype or the need of associated proteins, we investigated the subcellular localization of these titin fragments in C2C12 cells that had been differentiated for 7 d (Fig. 4 B). The differentiated myotubes displayed a typical cross-striated pattern that here was revealed by staining of obscurin and F-actin. Obscurin is positively correlated with progressive myoblast differentiation, and its cross-striated distribution is seen during the assembly of the myofibrillar contractile apparatus (Borisov et al., 2008). However, also in the 7 d

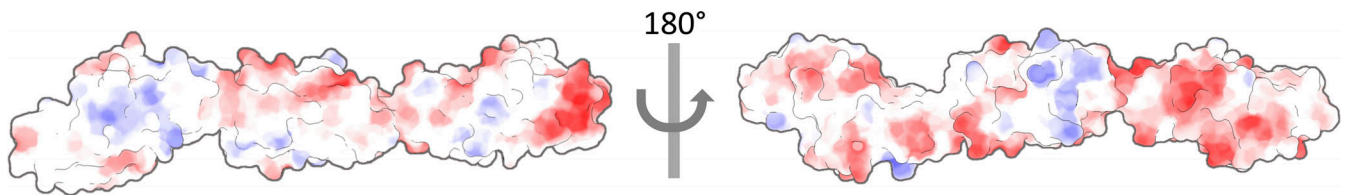


Figure 3. **Electrostatic surface potential of I81-I83.** Electrostatic potential energy at the I81-I83 protein surface reflecting charge distribution. The surface is colored by a gradient of potential energy values ranging from -15 kcal/mol.e (red) to $+15$ kcal/mol.e (blue; e is the charge of one electron).

differentiated cells, I80-UN2A-I81 and I81-I83 continued to display a diffuse cytoplasmic localization and did not form striations colocalized with actin that could be indicative of an interaction. Thus, no evidence could be obtained here for the association of the investigated titin N2A region with thin filaments.

Titin N2A components do not cosediment with F-actin in the presence or absence of calcium

To further study the lack of titin/F-actin association observed in C2C12 cells, we performed *in vitro* cosedimentation assays where titin UN2A-I81 and I81-I83 components were incubated with F-actin in the presence and absence of calcium (Fig. 5). Here, both UN2A-I81 and I81-I83 constructs were produced as recombinant samples in soluble form. Previous data on UN2A-I81 (Zhou et al., 2016) and the crystal structure of I81-I83 in this study demonstrate that the samples are monodisperse, stable, and structurally integral. Structural integrity and solubility are important considerations for this assay, as poorly folded proteins are prone to nonspecific interactions and aggregation, resulting in false positives.

In this assay, soluble protein samples that do not interact with actin remain in the supernatant fraction upon high-speed centrifugation ($100,000g$), while the large actin filaments sediment. Upon binding to F-actin, proteins that would otherwise remain in the soluble fraction after centrifugation will cosediment and appear in the pellet. In our control assays, we observed that single titin samples (in the absence of actin) show mild sedimentation behavior (Fig. 5). However, neither construct increases its basal level of sedimentation in the presence of F-actin, regardless of the presence or absence of calcium. Our cosedimentation data indicate that these titin-N2A segments do not associate with F-actin *in vitro*, thereby confirming the results in C2C12 cells.

Discussion

Titin N2A is a signaling hub that selectively recruits protein factors in the sarcomeric I-band. Proteins known to associate directly with N2A are MARPs, SMYD2, and P94/calpain3 (Hayashi et al., 2008; Miller et al., 2003; Lun et al., 2014; Voelkel

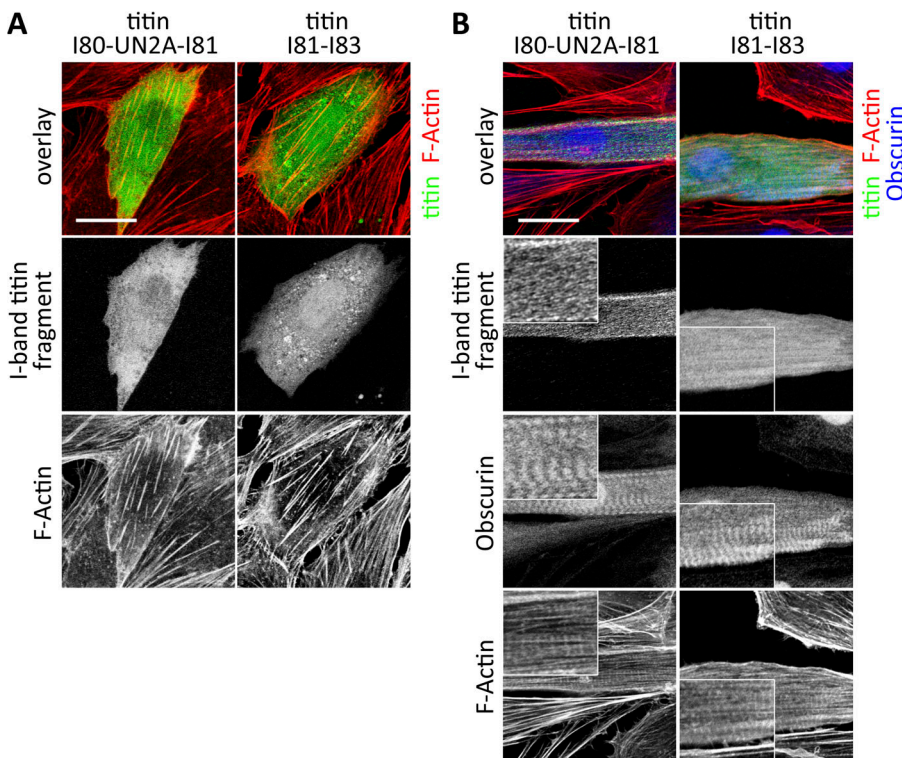


Figure 4. **Transfection of fluorescently tagged human titin constructs into C2C12 cells.** (A and B) Cells were transfected with constructs encoding titin GFP-I80-UN2A-I81 or mCherry-I81-I83. Undifferentiated cells (2 d, A; or 7 d, B) were transfected and counterstained with Alexa-647-phalloidin to visualize F-actin (red) and/or obscurin IQ-64 epitope antibody (Blondelle et al., 2019) to visualize obscurin (blue). Obscurin was used as a sarcomeric marker protein that localizes in a cross-striated pattern in mature, differentiated C2C12 myoblasts. Scale bar, $20\ \mu\text{m}$.

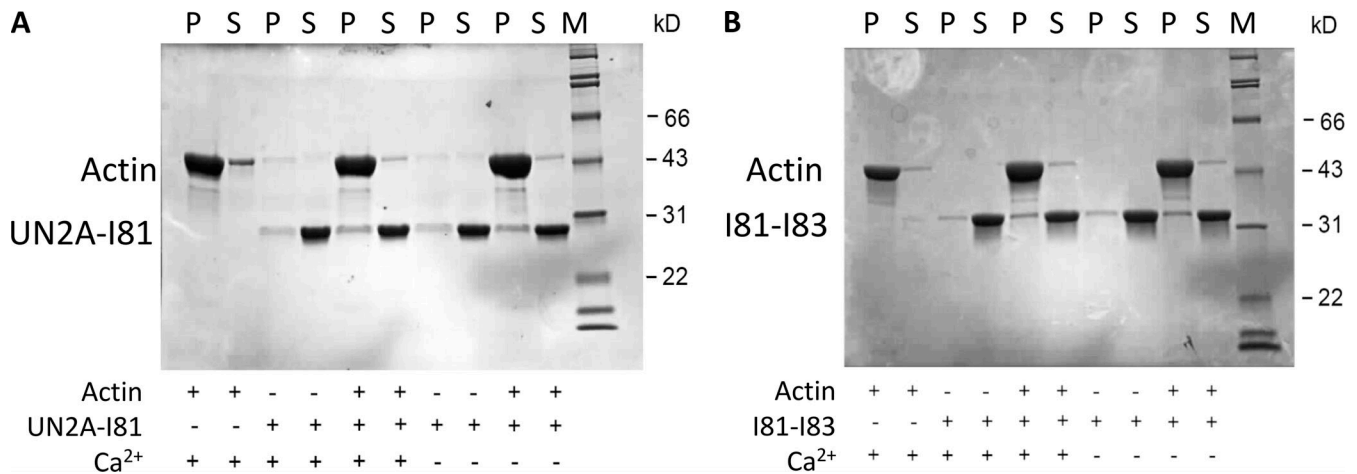


Figure 5. **F-actin cosedimentation of titin N2A components.** (A and B) F-actin cosedimentation of UN2A-I81 (A) and I81-I83 (B) in the presence and absence of calcium. No cosedimentation is observed in either the presence or absence of calcium. Lanes are labeled as follows: P, pelleted fraction; S, soluble fraction; M, molecular weight marker.

et al., 2013; Donlin et al., 2012), and further proteins known to associate through these proteins are HSP90 (Voelkel et al., 2013) and myopalladin (Fig. 6; Miller et al., 2003). Recently, a PKA phosphorylation target site has been found at the interface of the unique N2A sequence and domain I81 (Adams et al., 2019; Lanzicher et al., 2020), opening the possibility of a PKA-regulated formation of the N2A signalosome. Many interactions ascribed to titin N2A are mediated by its Ig components (Fig. 6). Notably, titin at its longest theoretical isoform contains 169 Ig domains in total (Bang et al., 2001). These Ig components are highly conserved, and their fold presents only small local differences, mostly in loop regions. Thus, the question remains of how Ig domains in I-band signaling hubs, such as N2A, can interact specifically with cellular binding partners, while most I-band Ig domains in titin are inert. The leading hypothesis is that to achieve binding specificity, domain components of titin's signaling loci have undergone (1) individualization as to display distinct local features in their fold. This fold diversification is often accompanied by (2) the development of multi-domain binding sites, where domains are packed serially along the titin chain with a distinct relative orientation that leads to a unique rotational architecture of the titin chain at that locus (Zacharchenko et al., 2015). These strategies are illustrated by the 3-D structures of the dual Ig-tandem Z1Z2 that binds telethonin in the Z-disc (Zou et al., 2006) and the A168-A170 tandem that recruits MuRF1 to M-line titin (Mrosek et al., 2007). The unique features of I81-I83, with its heterogeneous Ig components and distinct rotational chain order, further support this hypothesis. These findings confirm that the chain context of titin domains and the influence of loops and linkers on the chain architecture need to be considered to understand titin function in health and disease. For example, the analysis of inter-domain motions and features has been shown to be important when assessing the damage potential of single nucleotide variants (Bogomolovas et al., 2016; Fleming et al., 2020), with the recently developed Domain

Interface Score a useful parameter for assessing the damage potential of variants in linker regions (Fleming et al., 2020).

A prominent interacting partner proposed for N2A is F-actin (Dutta et al., 2018). This interaction is not expected to play a direct role in signaling, but to be of relevance for the mechanical regulation of the sarcomere (Dutta et al., 2018; Nishikawa et al., 2019, 2020). The hypothesized interaction of F-actin and titin N2A is thought to be enhanced by calcium (Dutta et al., 2018). Recent work showed that domain I83 has a notably reduced fold stability compared with I81 and I82, but that its stability increases in the presence of calcium (Kelly et al., 2020). This pointed to the possibility of I83 hosting a calcium-binding site, which could mediate a calcium-dependent association with actin. The elucidation of the crystal structure of I81-I83 in this work reveals the fold boundaries for these Ig domains, and sets the C terminus of I83 at residue T9851. By comparison, the N2A and I83 samples used in previous studies (Dutta et al., 2018; Kelly et al., 2020) were C-terminally truncated, missing three terminal residues in I83. The truncation compromised β -strand G that packs against β -strand A', sealing together the N and C termini of the domain fold. Truncations of just two to four terminal residues in titin Ig domains are known to result in notable domain destabilization, as exemplified by the truncations of M5 (Politou et al., 1994; Pfuhl et al., 1997) and I10 (Bogomolovas et al., 2016). It is thus possible that the instability of I83 previously reported might originate from the truncation of its β -strand G, even more so as I83 does not contain well-formed β -strands A and A' capping the β -strand G region. Furthermore, based on an analysis of the crystal structure, we found no molecular evidence for the existence of a specific calcium-binding site in I81-I83. This suggests that calcium effects on these Ig domains might be unspecific and result from the predominantly negatively charged surface of the domains, especially I83, which has the lowest pI value (pI = 5.05). This value is similar to that of Ig domain I27 (pI = 4.94), which is well characterized structurally and does not host specific metal-binding sites, but is stabilized by unspecific calcium interactions (DuVall et al., 2013).

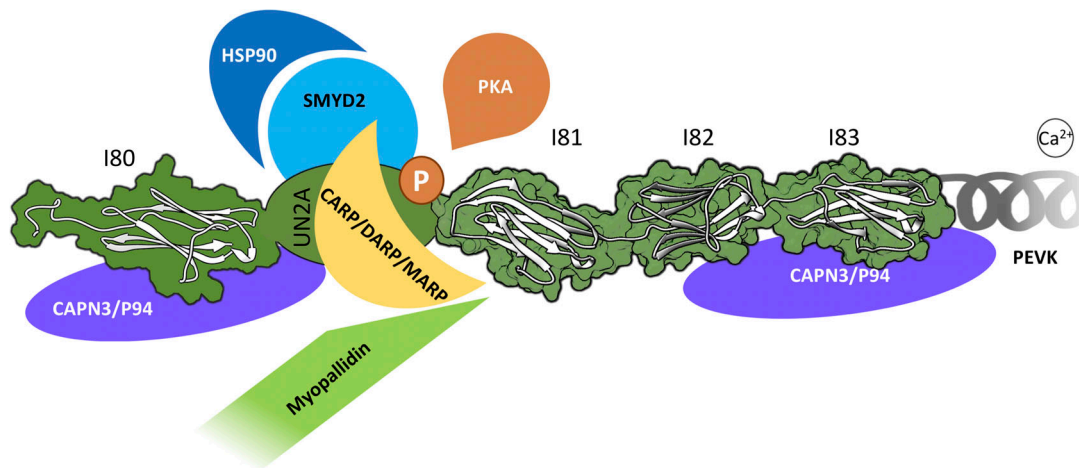


Figure 6. **N2A and its interaction partners.** Titin N2A is shown in forest green. The PEVK region is shown as a gray spring. Calcium is shown associated with PEVK. CAPN3/p94 (purple) associates with the I80-UN2A and I82-PEVK regions (Hayashi et al., 2008). MARPs (yellow) bind to UN2A-I81 (Zhou et al., 2016; Miller et al., 2003; Lun et al., 2014) and mediate the association of myopallidin to the node. SMYD2 localizes to UN2A and recruits HSP90 to N2A (Donlin et al., 2012). PKA (orange) phosphorylates S9578 in UN2A (Adams et al., 2019; Lanzicher et al., 2020).

Beyond the domain level, it cannot be ruled out, however, that a large-scale chain rearrangement could cause the creation of a cryptic metal binding site between domains, as observed in a highly infrequent conformation captured in the crystal structure of the Z-line titin tandem Z1Z2, where the domains fold onto themselves, forming a tight V shape stabilized by a metal ion sandwiched in between (Marino et al., 2006). Future studies will be required to explore the putative existence of such complex scenario.

In this work, we attempted to validate the N2A/F-actin interaction using both recombinant soluble samples *in vitro* and transfected C2C12 myoblasts. Under our experimental conditions, we did not observe an interaction between titin-N2A components and F-actin, independently of the presence or absence of calcium. The data show that I83 is not a critical mediator of actin binding. Our results agree with findings from an early study that assessed the competitive binding of the I79-I80-UN2A-I81-I82 segment to actin in the sarcomere by monitoring myofibril stiffness (Linke et al., 1997). However, our results did not concur with those of a recent study (Dutta et al., 2018) that used recombinant I80-UN2A-I81-I82-I83 extracted from insoluble inclusion bodies in cosedimentation studies. Inclusion body extraction is a difficult method to obtain soluble protein free of fold defects and without a tendency to aggregate unspecifically (Humer and Spadiut, 2018). In the actin cosedimentation assay reported (Dutta et al., 2018), the pelleting behavior of the isolated titin sample was not tested as a comparative control; therefore, the tendency of that sample to pellet and to associate unspecifically cannot be evaluated. Alternatively, a lack of cosedimentation in our work might result from the shorter length of our constructs or the absence of domain I80. However, the presence of I80, which has canonical structural features and lacks individualized elements, did not induce actin colocalization in C2C12-derived myotubes. Thus, this domain *per se* does not appear deterministic of

actin binding. Future investigations will be required to clarify the existence of a potential titin-N2A/F-actin interaction in the sarcomere.

In conclusion, our data reveal distinct features in titin N2A components that might underpin their selective role in signaling. However, the findings do not bring up evidence to support its proposed mediation in active force production through an association with actin.

Acknowledgments

Henk L. Granzier served as editor.

We acknowledge the Paul Scherrer Institut, Villigen, Switzerland, for provision of synchrotron radiation beamtime at beamline PX III of the Swiss Light Source, and would like to thank Dr. J. Wojdyla for assistance.

J.R. Fleming was supported by a European Union Marie Skłodowska-Curie Actions Individual Fellowship (TTNPred, 753054). O. Mayans acknowledges the financial support of the Leducq Foundation (TNE-13CVD04) and European Union RISE-H2020 “Muscle relief.” The work of S. Lange and E. Börgeson was supported by the National Institutes of Health (HL128457), the Swedish Hjärt-Lungfonden (20180199), the Marianne and Marcus Wallenberg Foundation, the Swedish Research Council (2016/82), the Swedish Society for Medical Research (S150086), and the European Research Council (804418). B. Bullard was supported by a grant from the Biotechnology and Biological Sciences Research Council (BB/M00676X/1).

The authors declare no competing financial interests.

Author contributions: J.R. Fleming and O. Mayans conceptualized and supervised the study; C. Stronczek performed cloning, protein production, and crystallization; S. Lange carried out cloning, C2C12 transfection, and imaging studies; and E. Börgeson assisted with imaging studies. J.R. Fleming, O. Mayans, and S. Wolniak performed crystallographic data analysis; B. Bullard performed actin cosedimentation assays. J.R. Fleming

and O. Mayans wrote the manuscript, and all authors made revisions.

Submitted: 30 September 2020

Accepted: 9 March 2021

References

- Adams, P.D., P.V. Afonine, G. Bunkóczi, V.B. Chen, I.W. Davis, N. Echols, J.J. Headd, L.-W. Hung, G.J. Kapral, R.W. Grosse-Kunstleve, et al. 2010. PHENIX: a comprehensive Python-based system for macromolecular structure solution. *Acta Crystallogr. D Biol. Crystallogr.* 66:213–221. <https://doi.org/10.1107/S0907444909052925>
- Adams, M., J.R. Fleming, E. Riehle, T. Zhou, T. Zacharchenko, M. Markovic, and O. Mayans. 2019. Scalable, Non-denaturing Purification of Phosphoproteins Using Ga³⁺-IMAC: N2A and MIM2 Titin Components as Study case. *Protein J.* 38:181–189. <https://doi.org/10.1007/s10930-019-09815-w>
- Bang, M.L., T. Centner, F. Fornoff, A.J. Geach, M. Gotthardt, M. McNabb, C.C. Witt, D. Labeit, C.C. Gregorio, H. Granzier, and S. Labeit. 2001. The complete gene sequence of titin, expression of an unusual approximately 700-kDa titin isoform, and its interaction with obscurin identify a novel Z-line to I-band linking system. *Circ. Res.* 89:1065–1072. <https://doi.org/10.1161/hh2301.100981>
- Blondelle, J., V. Marrocco, M. Clark, P. Desmond, S. Myers, J. Nguyen, M. Wright, S. Bremner, E. Pierantozzi, S. Ward, et al. 2019. Murine obscurin and Obsl1 have functionally redundant roles in sarcolemmal integrity, sarcoplasmic reticulum organization, and muscle metabolism. *Commun. Biol.* 2:178. <https://doi.org/10.1038/s42003-019-0405-7>
- Bogomolovas, J., J.R. Fleming, B.R. Anderson, R. Williams, S. Lange, B. Simon, M.M. Khan, R. Rudolf, B. Franke, B. Bullard, et al. 2016. Exploration of pathomechanisms triggered by a single-nucleotide polymorphism in titin's I-band: the cardiomyopathy-linked mutation T2580I. *Open Biol.* 6: 160114. <https://doi.org/10.1098/rsob.160114>
- Borisov, A.B., M.Ö. Raeker, and M.W. Russell. 2008. Developmental expression and differential cellular localization of obscurin and obscurin-associated kinase in cardiac muscle cells. *J. Cell. Biochem.* 103:1621–1635. <https://doi.org/10.1002/jcb.21551>
- Cazorla, O., A. Freiburg, M. Helmes, T. Centner, M. McNabb, Y. Wu, K. Trombitás, S. Labeit, and H. Granzier. 2000. Differential expression of cardiac titin isoforms and modulation of cellular stiffness. *Circ. Res.* 86: 59–67. <https://doi.org/10.1161/01.RES.86.1.59>
- Cazorla, O., Y. Wu, T.C. Irving, and H. Granzier. 2001. Titin-based modulation of calcium sensitivity of active tension in mouse skinned cardiac myocytes. *Circ. Res.* 88:1028–1035. <https://doi.org/10.1161/hh1001.090876>
- Donlin, L.T., C. Andresen, S. Just, E. Rudensky, C.T. Pappas, M. Kruger, E.Y. Jacobs, A. Unger, A. Ziesenis, M.-W. Dobenecker, et al. 2012. Smyd2 controls cytoplasmic lysine methylation of Hsp90 and myofibrillar organization. *Genes Dev.* 26:114–119. <https://doi.org/10.1101/gad.17758.111>
- Dutta, S., C. Tsiros, S.L. Sundar, H. Athar, J. Moore, B. Nelson, M.J. Gage, and K. Nishikawa. 2018. Calcium increases titin N2A binding to F-actin and regulated thin filaments. *Sci. Rep.* 8:14575. <https://doi.org/10.1038/s41598-018-32952-8>
- DuVall, M.M., J.L. Gifford, M. Amrein, and W. Herzog. 2013. Altered mechanical properties of titin immunoglobulin domain 27 in the presence of calcium. *Eur. Biophys. J.* 42:301–307. <https://doi.org/10.1007/s00249-012-0875-8>
- Emsley, P., and K. Cowtan. 2004. Coot: model-building tools for molecular graphics. *Acta Crystallogr. D Biol. Crystallogr.* 60:2126–2132. <https://doi.org/10.1107/S0907444904019158>
- Fleming, J.R., D.J. Rigden, and O. Mayans. 2020. The importance of chain context in assessing small nucleotide variants in titin: *in silico* case study of the I10-I11 tandem and its arrhythmic right ventricular cardiomyopathy linked position T2580. *J. Biomol. Struct. Dyn.*:1–11. <https://doi.org/10.1080/07391102.2020.1768148>
- Fleming, J. 2021. Images for titin-N2A Ig81-Ig83 pdb 7HAS Zenodo. <https://doi.org/10.5281/zenodo.4045608>
- Garvey, S.M., C. Rajan, A.P. Lerner, W.N. Frankel, and G.A. Cox. 2002. The muscular dystrophy with myositis (mdm) mouse mutation disrupts a skeletal muscle-specific domain of titin. *Genomics.* 79:146–149. <https://doi.org/10.1006/geno.2002.6685>
- Granzier, H.L., and S. Labeit. 2004. The giant protein titin: a major player in myocardial mechanics, signaling, and disease. *Circ. Res.* 94:284–295. <https://doi.org/10.1161/01.RES.0000117769.88862.F8>
- Hayashi, C., Y. Ono, N. Doi, F. Kitamura, M. Tagami, R. Mineki, T. Arai, H. Taguchi, M. Yanagida, S. Hirner, et al. 2008. Multiple molecular interactions implicate the connectin/titin N2A region as a modulating scaffold for p94/calpain 3 activity in skeletal muscle. *J. Biol. Chem.* 283: 14801–14814. <https://doi.org/10.1074/jbc.M708262200>
- Henderson, C.A., C.G. Gomez, S.M. Novak, L. Mi-Mi, and C.C. Gregorio. 2017. Overview of the muscle cytoskeleton. *Compr. Physiol.* 7:891–944. <https://doi.org/10.1002/cphy.c160033>
- Hessel, A.L., S.L. Lindstedt, and K.C. Nishikawa. 2017. Physiological Mechanisms of Eccentric Contraction and Its Applications: A Role for the Giant Titin Protein. *Front. Physiol.* 8:70. <https://doi.org/10.3389/fphys.2017.00070>
- Hu, X., Q. Dong, J. Yang, and Y. Zhang. 2016. Recognizing metal and acid radical ion-binding sites by integrating ab initio modeling with template-based transfers. *Bioinformatics.* 32:3260–3269. <https://doi.org/10.1093/bioinformatics/btw396>
- Huebsch, K.A., E. Kudryashova, C.M. Wooley, R.B. Sher, K.L. Seburn, M.J. Spencer, and G.A. Cox. 2005. Mdm muscular dystrophy: interactions with calpain 3 and a novel functional role for titin's N2A domain. *Hum. Mol. Genet.* 14:2801–2811. <https://doi.org/10.1093/hmg/ddi313>
- Humer, D., and O. Spadiut. 2018. Wanted: more monitoring and control during inclusion body processing. *World J. Microbiol. Biotechnol.* 34:158. <https://doi.org/10.1007/s11274-018-2541-5>
- Kabsch, W. 2010. Software XDS for image rotation, recognition and crystal symmetry assignment. *Acta Crystallogr. D Biol. Crystallogr.* 66:125–132. <https://doi.org/10.1107/S0907444909047337>
- Katz, A.K., J.P. Glusker, S.A. Beebe, and C.W. Bock. 1996. Calcium ion coordination: A comparison with that of beryllium, magnesium, and zinc. *J. Am. Chem. Soc.* 118:5752–5763. <https://doi.org/10.1021/ja953943i>
- Kellermayer, M.S.Z., and H.L. Granzier. 1996. Calcium-dependent inhibition of *in vitro* thin-filament motility by native titin. *FEBS Lett.* 380:281–286. [https://doi.org/10.1016/0014-5793\(96\)00055-5](https://doi.org/10.1016/0014-5793(96)00055-5)
- Kelley, L.A., S. Mezulis, C.M. Yates, M.N. Wass, and M.J.E. Sternberg. 2015. The Phyre2 web portal for protein modeling, prediction and analysis. *Nat. Protoc.* 10:845–858. <https://doi.org/10.1038/nprot.2015.053>
- Kelly, C.M., S. Manukian, E. Kim, and M.J. Gage. 2020. Differences in stability and calcium sensitivity of the Ig domains in titin's N2A region. *Protein Sci.* 29:1160–1171. <https://doi.org/10.1002/pro.3848>
- Labeit, D., K. Watanabe, C. Witt, H. Fujita, Y. Wu, S. Lahmers, T. Funck, S. Labeit, and H. Granzier. 2003. Calcium-dependent molecular spring elements in the giant protein titin. *Proc. Natl. Acad. Sci. USA.* 100: 13716–13721. <https://doi.org/10.1073/pnas.2235652100>
- Lamzin, V.S., A. Perrakis, and K.S. Wilson. 2012. ARP/wARP – automated model building and refinement. In *International Tables for Crystallography*. C.P. Brock, T. Hahn, H. Wondratschek, U. Müller, U. Shmueli, E. Prince, A. Authier, V. Kopský, D.B. Litvin, E. Arnold, et al. editors. Wiley, Hoboken, New Jersey. <https://doi.org/10.1107/97809553602060000862>
- Lange, S., S. Perera, P. Teh, and J. Chen. 2012. Obscurin and KCTD6 regulate cullin-dependent small ankyrin-1 (sAnk1.5) protein turnover. *Mol. Biol. Cell.* 23:2490–2504. <https://doi.org/10.1091/mbc.e12-01-0052>
- Lanzicher, T., T. Zhou, C. Saripalli, V. Keschrumrus, J.E. Smith III, O. Mayans, O. Sbaizero, H. Granzier. 2020. Single-Molecule Force Spectroscopy on the N2A Element of Titin: Effects of Phosphorylation and CARP. *Front. Physiol.* 11:173. <https://doi.org/10.3389/fphys.2020.00173>
- Lee, E.J., J. Nedrud, P. Schemmel, M. Gotthardt, T.C. Irving, and H.L. Granzier. 2013. Calcium sensitivity and myofibrillar lattice structure in titin N2B KO mice. *Arch. Biochem. Biophys.* 535:76–83. <https://doi.org/10.1016/j.abb.2012.12.004>
- LeWinter, M.M., and H. Granzier. 2010. Cardiac titin: a multifunctional giant. *Circulation.* 121:2137–2145. <https://doi.org/10.1161/CIRCULATIONAHA.109.860171>
- Linke, W.A., M. Ivemeyer, S. Labeit, H. Hinssen, J.C. Rüegg, and M. Gautel. 1997. Actin-titin interaction in cardiac myofibrils: probing a physiological role. *Biophys. J.* 73:905–919. [https://doi.org/10.1016/S0006-3495\(97\)78123-2](https://doi.org/10.1016/S0006-3495(97)78123-2)
- Lun, A.S., J. Chen, and S. Lange. 2014. Probing muscle ankyrin-repeat protein (MARP) structure and function. *Anat. Rec. (Hoboken).* 297:1615–1629. <https://doi.org/10.1002/ar.22968>
- Marino, M., D.I. Svergun, L. Kreplak, P.V. Konarev, B. Maco, D. Labeit, and O. Mayans. 2005. Poly-Ig tandems from I-band titin share extended domain arrangements irrespective of the distinct features of their modular constituents. *J. Muscle Res. Cell Motil.* 26:355–365.
- Marino, M., P. Zou, D. Svergun, P. Garcia, C. Edlich, B. Simon, M. Wilmanns, C. Muhle-Goll, and O. Mayans. 2006. The Ig doublet Z1Z2: a model system for the hybrid analysis of conformational dynamics in Ig tandems from titin. *Structure.* 14:1437–1447. <https://doi.org/10.1016/j.str.2006.07.009>

- McCoy, A.J., R.W. Grosse-Kunstleve, P.D. Adams, M.D. Winn, L.C. Storoni, and R.J. Read. 2007. Phaser crystallographic software. *J. Appl. Cryst.* 40: 658–674. <https://doi.org/10.1107/S0021889807021206>
- Miller, M.K., M.-L.L. Bang, C.C. Witt, C. Trombitas, K. Watanabe, H. Granzier, A.S. McElhinny, C.C. Gregorio, and S. Labeit. 2003. The muscle ankyrin repeat proteins: CARP, ankrd2/Arpp and DARP as a family of titin filament-based stress response molecules. *J. Mol. Biol.* 333:951–964. <https://doi.org/10.1016/j.jmb.2003.09.012>
- Mrosek, M., D. Labeit, S. Witt, H. Heerklotz, E. von Castelmur, S. Labeit, and O. Mayans. 2007. Molecular determinants for the recruitment of the ubiquitin-ligase MuRF-1 onto M-line titin. *FASEB J.* 21:1383–1392. <https://doi.org/10.1096/fj.06-7644com>
- Nishikawa, K., S. Dutta, M. DuVall, B. Nelson, M.J. Gage, and J.A. Monroy. 2019. Calcium-dependent titin–thin filament interactions in muscle: observations and theory. *J. Muscle Res. Cell Motil.* •••:1–15. <https://doi.org/10.1007/s10974-019-09540-y>
- Nishikawa, K., S.L. Lindstedt, A. Hessel, and D. Mishra. 2020. N2A titin: Signaling hub and mechanical switch in skeletal muscle. *Int. J. Mol. Sci.* 21:3974. <https://doi.org/10.3390/ijms21113974>
- Pettersen, E.F., T.D. Goddard, C.C. Huang, G.S. Couch, D.M. Greenblatt, E.C. Meng, and T.E. Ferrin. 2004. UCSF Chimera—a visualization system for exploratory research and analysis. *J. Comput. Chem.* 25:1605–1612. <https://doi.org/10.1002/jcc.20084>
- Pfuhl, M., S. Improta, A.S. Politou, and A. Pastore. 1997. When a module is also a domain: the rôle of the N terminus in the stability and the dynamics of immunoglobulin domains from titin. *J. Mol. Biol.* 265:242–256. <https://doi.org/10.1006/jmbi.1996.0725>
- Politou, A.S., M. Gautel, M. Pfuhl, S. Labeit, and A. Pastore. 1994. Immunoglobulin-type domains of titin: same fold, different stability? *Biochemistry.* 33:4730–4737. <https://doi.org/10.1021/bi00181a604>
- Powers, K., K. Nishikawa, V. Joumaa, and W. Herzog. 2016. Decreased force enhancement in skeletal muscle sarcomeres with a deletion in titin. *J. Exp. Biol.* 219:1311–1316. <https://doi.org/10.1242/jeb.132027>
- Sodhi, J.S., K. Bryson, L.J. McGuffin, J.J. Ward, L. Wernisch, and D.T. Jones. 2004. Predicting metal-binding site residues in low-resolution structural models. *J. Mol. Biol.* 342:307–320. <https://doi.org/10.1016/j.jmb.2004.07.019>
- Spudich, J.A., and S. Watt. 1971. The regulation of rabbit skeletal muscle contraction. I. Biochemical studies of the interaction of the tropomyosin-troponin complex with actin and the proteolytic fragments of myosin. *J. Biol. Chem.* 246:4866–4871. [https://doi.org/10.1016/S0021-9258\(18\)62016-2](https://doi.org/10.1016/S0021-9258(18)62016-2)
- Tahir, U., J.A. Monroy, N.A. Rice, and K.C. Nishikawa. 2020. Effects of a titin mutation on force enhancement and force depression in mouse soleus muscles. *J. Exp. Biol.* 223:jeb197038. <https://doi.org/10.1242/jeb.197038>
- Tiffany, H., K. Sonkar, and M.J. Gage. 2017. The insertion sequence of the N2A region of titin exists in an extended structure with helical characteristics. *Biochim. Biophys. Acta. Proteins Proteomics.* 1865:1–10. <https://doi.org/10.1016/j.bbapap.2016.10.003>
- Trombitás, K., M. Greaser, S. Labeit, J.P. Jin, M. Kellermayer, M. Helmes, and H. Granzier. 1998. Titin extensibility in situ: entropic elasticity of permanently folded and permanently unfolded molecular segments. *J. Cell Biol.* 140:853–859. <https://doi.org/10.1083/jcb.140.4.853>
- Voelkel, T., C. Andresen, A. Unger, S. Just, W. Rottbauer, and W.A. Linke. 2013. Lysine methyltransferase Smyd2 regulates Hsp90-mediated protection of the sarcomeric titin springs and cardiac function. *Biochim. Biophys. Acta.* 1833:812–822. <https://doi.org/10.1016/j.bbamcr.2012.09.012>
- von Castelmur, E., M. Marino, D.I. Svergun, L. Kreplak, Z. Ucurum-Fotiadis, P.V. Konarev, A. Urzhumtsev, D. Labeit, S. Labeit, and O. Mayans. 2008. A regular pattern of Ig super-motifs defines segmental flexibility as the elastic mechanism of the titin chain. *Proc. Natl. Acad. Sci. USA.* 105: 1186–1191. <https://doi.org/10.1073/pnas.0707163105>
- Williams, C.J., J.J. Headd, N.W. Moriarty, M.G. Prisant, L.L. Videau, L.N. Deis, V. Verma, D.A. Keedy, B.J. Hintze, V.B. Chen, et al. 2018. MolProbity: More and better reference data for improved all-atom structure validation. *Protein Sci.* 27:293–315. <https://doi.org/10.1002/pro.3330>
- Witt, C.C., Y. Ono, E. Puschmann, M. McNabb, Y. Wu, M. Gotthardt, S.H. Witt, M. Haak, D. Labeit, C.C. Gregorio, et al. 2004. Induction and myofibrillar targeting of CARP, and suppression of the Nkx2.5 pathway in the MDM mouse with impaired titin-based signaling. *J. Mol. Biol.* 336: 145–154. <https://doi.org/10.1016/j.jmb.2003.12.021>
- Yamasaki, R., M. Berri, Y. Wu, K. Trombitás, M. McNabb, M.S.Z. Kellermayer, C. Witt, D. Labeit, S. Labeit, M. Greaser, and H. Granzier. 2001. Titin-actin interaction in mouse myocardium: passive tension modulation and its regulation by calcium/S100A1. *Biophys. J.* 81:2297–2313. [https://doi.org/10.1016/S0006-3495\(01\)75876-6](https://doi.org/10.1016/S0006-3495(01)75876-6)
- Yang, J., and Y. Zhang. 2015. I-TASSER server: new development for protein structure and function predictions. *Nucleic Acids Res.* 43(W1): W174–W181. <https://doi.org/10.1093/nar/gkv342>
- Yang, J., A. Roy, and Y. Zhang. 2013. BioLiP: a semi-manually curated database for biologically relevant ligand-protein interactions. *Nucleic Acids Res.* 41(Database issue, D1):D1096–D1103. <https://doi.org/10.1093/nar/gks966>
- Zacharchenko, T., E. von Castelmur, D.J. Rigden, and O. Mayans. 2015. Structural advances on titin: towards an atomic understanding of multi-domain functions in myofilament mechanics and scaffolding. *Biochem. Soc. Trans.* 43:850–855. <https://doi.org/10.1042/BST20150084>
- Zhou, T., J.R. Fleming, B. Franke, J. Bogomolovas, I. Barsukov, D.J. Rigden, S. Labeit, and O. Mayans. 2016. CARP interacts with titin at a unique helical N2A sequence and at the domain Ig81 to form a structured complex. *FEBS Lett.* 590:3098–3110. <https://doi.org/10.1002/1873-3468.12362>
- Zou, P., N. Pinotsis, S. Lange, Y.-H. Song, A. Popov, I. Mavridis, O.M. Mayans, M. Gautel, and M. Wilmanns. 2006. Palindromic assembly of the giant muscle protein titin in the sarcomeric Z-disk. *Nature.* 439:229–233. <https://doi.org/10.1038/nature04343>